YAG-MIG 复合焊接 5A90 等离子体光谱分析与温度计算

国 莉[1,2]， 段爱琴[2]， 于有生[1]

（1. 武汉理工大学 材料科学与工程学院，武汉 430070；
2. 北京航空制造工程研究所 高能束流加工技术国防科技重点实验室，北京 100024）

摘 要：5A90 铝锂合金在航空航天中的重要应用使得对其焊接性的研究变得尤为重要. 在 YAG-MIG 复合焊接 5A90 的条件下，使用光谱仪对焊接过程中金属蒸气/等离子体进行监测，获得了其特征光谱分布，并由谱线相对强度法计算获得了金属蒸气/等离子体的温度，并对焊接工艺参数对金属蒸气/等离子体温度的影响进行了探讨. 结果表明，复合焊接的特征光谱在 350～850 nm 范围内以大量的高强度的氩离子谱线为主，伴有少量镁、锂离子. 得到了一组工艺参数下复合焊接 5A90 过程中等离子体的平均温度为 6 554 K，比同等工艺参数水平下 YAG 焊的增加了将近 1 200 K，而与电弧焊的比较接近.

关键词：YAG-MIG 复合焊接；金属蒸气/等离子体；光谱监测
中图分类号：TG422.3 文献标识码：A 文章编号：0253－360X(2009)03－0106－03

国 莉

0 序 言

铝锂合金具有低密度高比强度等特点，是航空航天工业中理想的结构材料. 但熔焊时易产生热裂纹、易形成气孔，并且接头存在一定宽度的弱化区，影响了在焊接领域的应用. 激光焊接能量密度高、加热速度快，很大程度上克服上述缺陷，但是它对装配间隙和对位精度的高要求限制了其应用. 而激光电弧复合焊的出现可以有效地解决上述问题，既保留激光焊接变形小、精度高等优点，又通过引入电弧来改善接头的力学性能、消除气孔和裂纹等焊接缺陷并降低激光焊接对装配间隙和对位精度的要求，很好地实现了两种热源的优势互补.

激光与电弧的相互作用十分复杂，研究金属蒸气/等离子体的物理特性以探讨激光电弧复合焊接两热源相互作用机理. 国内外很多学者做过激光焊接中金属蒸气/等离子体温度测量. Duchamne 等人[1] 测得孔内等离子体的温度可以达到 19 000 ℃，Finke 等人[2] 基于弱电离等离子体的假设上建立了一个简单的数学模型，估算小孔孔内等离子体的平均电子温度为 8 500 K. Mutsunawa 等人[3] 在 YAG 焊接 Al-Mg 合金时得到的等离子体的温度为 3 280 K 左右. 但是目前对于复合焊接铝锂合金中等离子体的研究还很少. 文中针对 5A90 铝锂合金的 YAG-MIG 复合焊接，研究了其特征光谱分布并计算了金属蒸气/等离子体的温度.

收稿日期：2008－09－01
基金项目：国防预研基金资助项目

1 试验方法

激光与电弧热源分别采用 3 kW 的 YAG 激光器和福尼斯公司生产的 TPS4000 直流脉冲电源，使用 Acton Research Corporation 的 Spectra Pro－500i 光谱仪及 Princeton instrument 公司的 ST133 光谱仪控制器对焊接过程产生的金属蒸气/等离子体进行光谱监测.

试验材料 5A90 是一种中强度焊接性的铝锂合金. 其化学成分（质量分数，%）为 Al＞90.8，Mg 5.0～6.0，Li 1.9～2.3，Zr 0.1～0.5，Fe＜0.2，Si＜0.1，H＜0.1.

2 试验理论与计算方法

目前，测量激光光致等离子体温度的方法有谱线的绝对强度法、相对强度法、玻尔兹曼图法、谱线轮廓法等. 谱线相对强度法可以不需要知道配分函数，只需要测量等离子体的两条谱线的相对强度，查

出两条谱线的跃迁几率和统计权重等相关信息, 就可以求得等离子体温度, 并且该方法具有较高的测量精度. 综合各种方法的优缺点及文中的实际情况, 文中选用谱线相对强度法[4] 来计算小孔外等离子体的温度.

在局部热力学平衡下, 为了估计等离子体温度, 测量两种波长 λ_p 和 λ_s 的谱线强度, 将玻尔兹曼分布分别代入两条谱线的强度公式并求比, 可得等离子体温度为

$$T_s(k) = \frac{5\,040(E_s - E_p)}{\log[\frac{g_s A_{sq}}{g_p A_{pq}}] - \log[\frac{\lambda_s}{\lambda_p}] - \log[\frac{I_{sq}}{I_{pq}}]} \quad (1)$$

式中: T_e 为等离子体温度, 单位为 K; E_s, E_p 分别为高能态(s 态) 与低能态(p 态) 的能量; g_s, g_p 为简并度; A_{sq}, A_{pq} 为跃迁几率, 均可查表获得; I_{sq}, I_{pq} 为试验测量值.

3　试验结果与分析

3.1　YAG-MIG 复合焊接 5A90 的特征光谱分布

图 1 为 5A90 铝锂合金的 YAG-MIG 激光电弧复合焊接在 250 ~ 850 nm 波长范围内的特征光谱分布. 由图可见, 在 250 ~ 350 nm 段, 其特征光谱以相对光谱强度较低的连续谱为主, 而在 350 ~ 850 nm 整个可见光至近红外区域内, 其特征光谱则以大量的氩离子谱线为主, 伴有少数几条 Mg, Li 谱线, 如 Mg Ⅰ 552.8, Li Ⅰ 670.8 等. 整体的相对光谱强度也均在 60 000 以上.

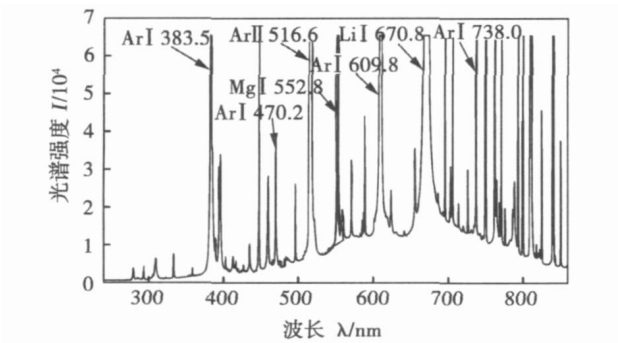

图 1　YAG-MIG 复合焊接 5A90 的特征光谱分布

Fig. 1　Typical spectrum distribution of YAG-MIG hybrid welding of 5A90

对比同等参数水平下的 YAG 激光焊接, 如图 2a 所示. 可以看出, 在 550 ~ 850 nm 波长范围内, YAG 激光焊接 5A90 的特征光谱只有稀疏的几条以锂、镁、氩离子为主的线光谱, 而且整体谱线相对强度远低于复合焊接时, 只有 Li Ⅰ 670.8 的相对强度达到了 20 000, 且远高于其它谱线.

对比同等参数水平下的 MIG 电弧焊接, 如图 2b 所示, 很明显二者的光谱分布比较相似, 都是以高的相对光谱强度的氩离子的线光谱为主, 但是复合焊在激光与电弧的共同作用下, 其光谱仍然发生了不小的变化, 如出现了 Ar Ⅰ 609.8 等新的谱线. 因而说明这两个过程中电离还是发生了变化, 尽管激光时电离程度很低, 但它在复合焊中对金属蒸气/等离子体的作用非常明显, 且不同于激光焊.

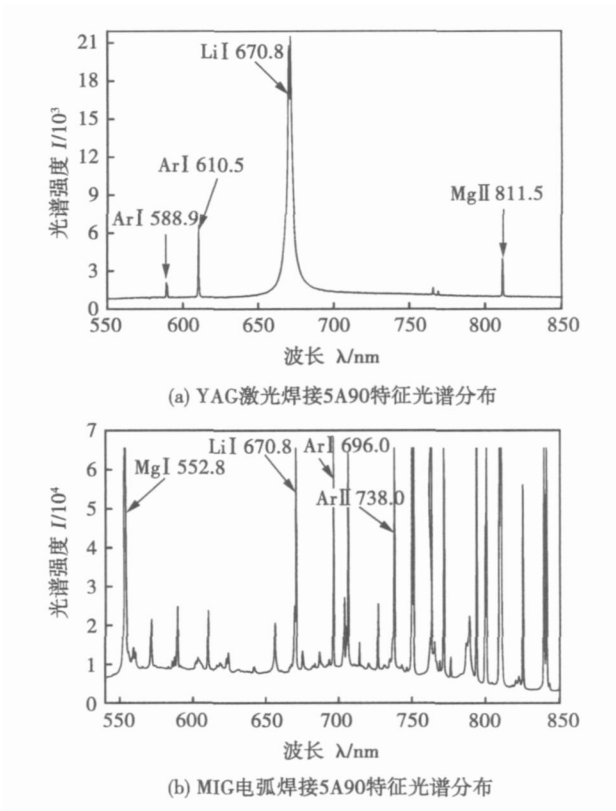

图 2　YAG 激光、MIG 电弧焊接 5A90 的特征光谱分布

Fig. 2　Typical spectra distribution of YAG welding and MIG welding of 5A90

3.2　YAG-MIG 复合焊接 5A90 金属蒸气/等离子体的温度

图 3 为相同工艺参数水平下, 复合焊接与 YAG 焊接、MIG 电弧焊接的平均温度的对比曲线. 可以看出, 在同等工艺参数条件下, 复合焊接由于引入了电弧, 其等离子体的平均温度比 YAG 焊时(其平均温度为 5 425 K) 增加了将近 1 200 K, 而此温度与电弧焊时(其平均温度为 6 749 K) 比较接近.

在 YAG 激光焊接 5A90 铝锂合金中的等离子体主要以 Mg, Li 等轻质合金元素为主的稀薄的金属蒸气/等离子体, 如图 2a 所示. Mg, Li 由于其低的汽化温度(Mg, Li 的沸点分别为 1 380, 1 590 K) 及低的电

离能(Mg, Li 的电离能分别为 7.65 eV, 5.39 eV)而容易电离并形成等离子体, 故以 Mg, Li 元素为主的金属蒸气/等离子体的温度较低. 而电弧的加入一方面使输入能量增加, 另一方面, 大量氩弧等离子体的产生改变了原来的金属蒸气/等离子体的组成, 如图 1 所示, 复合焊接中的金属蒸气/等离子体为以氩弧等离子体为主的致密等离子体.

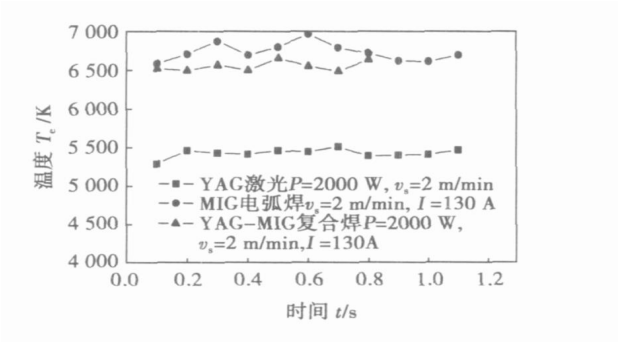

图 3 5A90 复合焊接等离子体温度与激光焊、电弧焊的对比

Fig. 3 Temperature comparison between YAG-MIG hybrid welding and laser welding and arc welding of 5A90 alloy

3.3 焊接工艺参数对 YAG-MIG 复合焊接中金属蒸气/等离子体温度的影响

文中试验条件下 YAG-MIG 复合焊接的主要工艺参数为电弧电流、激光功率、焊接速度. 根据测量与计算, 获得了不同电弧电流下金属蒸气/等离子体温度的变化曲线, 如图 4. 经计算, 在激光功率 1 800 W, 焊接速度 2 m/min 的条件下, 当电弧电流分别为 110, 120, 130, 140 A 的时候, 其等离子体的平均温度分别为 6 810, 6 704, 6 605, 6 449 K. 可以看出, 随着电弧电流的增加, 金属蒸气/等离子体的温度呈逐渐降低的趋势, 但是变化幅度很小.

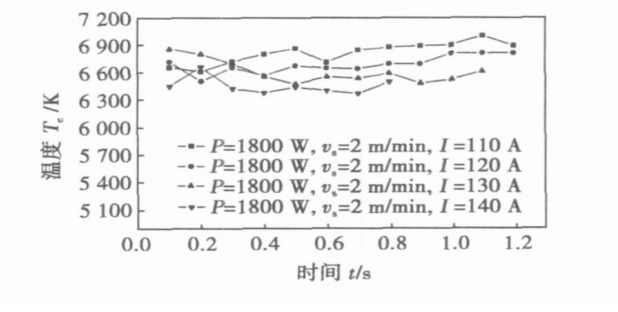

图 4 电弧电流对温度的影响

Fig. 4 Effect of arc current on electron temperature

图 5 为不同激光热输入下金属蒸气/等离子体温度的变化曲线. 在电弧电流为 130 A 的条件下, 当热输入从 43 J/mm 增加到 60 J/mm 时, 金属蒸气/等离子体的平均温度从 6 393 ~6 554 K 之间变化, 呈逐渐上升趋势, 但是变化幅度仍然很小. 可见, 焊接工艺参数对 YAG-MIG 复合焊接中金属蒸气/等离子体温度的影响不大.

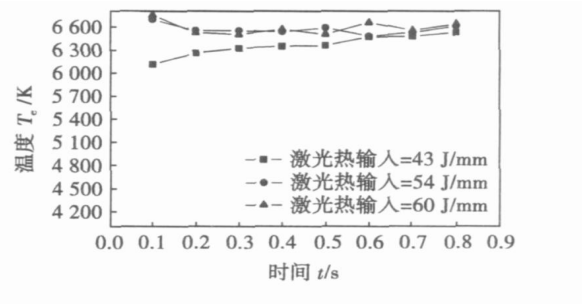

图 5 热输入对温度的影响

Fig. 5 Effect of heat input on electron temperature

4 结 论

(1) 复合焊接的特征光谱在 350 ~850 nm 范围内以大量的氩离子谱线为主, 伴有少量镁、锂离子, 并且整体相对光谱强度均达到 60 000 以上.

(2) 在文中焊接条件下, 复合焊接 5A90 等离子体的平均温度为 6 554 K, 比同等工艺参数水平下 YAG 焊时(其平均温度为 5 425 K)增加了将近 1 200 K, 而与电弧焊时(其平均温度为 6 749 K)比较接近.

(3) 焊接工艺参数对 YAG-MIG 复合焊接中金属蒸气/等离子体温度的影响不大. 电弧电流由 110 A 增加至 140 A 时, 金属蒸气/等离子体平均温度从 6 810 K变化到 6 449 K, 呈逐渐降低的趋势, 但是变化幅度很小. 激光热输入从 43 ~60 J/mm 之间变化时, 金属蒸气/等离子体平均温度从 6 393 K 变化到 6 554 K, 呈逐渐上升趋势, 但是变化幅度也很小.

参考文献:

[1] Ducharme R, Williams K, Kapadia P D, *et al*. The laser welding of thin metal sheets: an integrated keyhole and weld pool model with supporting experiments[J]. Journal of Physics D: Applied Physics 27, 1994: 1619—1627.

[2] Finke B R, Kapadiat P D, Dowden J M. A fundamental plasma based model for energy transfer in laser material processing[J]. Journal of Physics D: Applied Physics, 1990, 23: 643—654.

[3] Matsunawa A, Kim J D, Takemoto T, *et al*. Spectroscopic studies on laser induced plume of aluminum alloys[J]. ICALEO, 1995 Congress Proceeding, 171—172.

[4] Duley W W. Laser welding[M]. New York, 1998.

作者简介: 国 莉, 女, 1984 年出生, 硕士. 从事激光焊接光谱监测方面的研究.

Email: monica84315@163.com

posite bonds increases by 50% than that of the brazed bond without SiC particles. The increased strength is associated with the increase of the aluminum content and the quantity of reinforcement particles in the bond metal.

Key words: aluminum matrix composites; ultrasonically aided brazing; shear strength; microstructure; formation of composite joint

Model of forces on pin tool and its application ZHOU Li, LIU Huijie, LIU Peng (National Key Laboratory of Advanced Welding Production Technology, Harbin Institute of Technology, Harbin 150001, China). p93—96

Abstract: A model of forces on pin tool in the plunge stage and the steady welding stage during the friction stir welding (FSW) process is established and verified by comparison with experimental data. It indicates that pin root is the weakest portion of the pin tool in either the plunge stage or the steady welding stage. Pin tool can fail from the root if improper design is adopted, so the model is applied to guide design of tools for FSW of Ti-6Al-4V. The results show that proper tool design is vital to FSW for Ti-6Al-4V. Sound welds could be obtained under appropriate parameters.

Key words: friction stir welding; pin tool; model of force; Ti-6Al-4V

Characteristics of DC TIG arc with the action of a vertically incident CO_2 laser beam ZHANG Huanzhen, WU Shikai, XIAO Rongshi (Institute of Laser Engineering, Beijing University of Technology, Beijing 100022, China). p97—100

Abstract: Laser-arc hybrid welding is one of the advanced joining techniques. By using instruments such as a high-speed camera and a laser power meter, the effects of a vertically incident CO_2 laser beam on characteristics of a DC tungsten inter-gas arc are investigated. Results demonstrate that the laser-arc interaction causes the curve of arc static characteristic to shift downwards, the arc column to expand, the electric power to decease and the total arc power increase. With the increase of the laser power, the downward shift of the static characteristic curve increases, but the total arc power increases. The lower the arc current is and the nearer the laser beam locates to the cathode, the more the arc voltage decreases, which the expansion of the arc column mainly occurs in the range between the laser beam location and the anode.

Key words: tungsten inter-gas; CO_2 laser; static characteristic of arc; arc configuration; arc power

Fatigue analysis of welded joints by method of structural stress WU Qi, QIU Huiqing, WANG Weisheng (Department of Mechanical Engineering, Tongji University, Shanghai 201804, China). p101—105

Abstract: Based on the structural stress method, some data of the fatigue strength of 16Mn, which include non-carrying-load fillet cruciform joints, carrying-load fillet cruciform joints and welded joints with longitudinal fillet welded gusset, are analyzed. The discrete structural stress formula which suits for finite element method are deduced, structural stress concentration factors for joints are obtained, and structural S-N curves for these joints are provided. The approach shows the good mesh-size insensitive characteristics. Compared with the nominal stress method, the dispersity of experimental data evaluated by structural stress method is reduced.

Key words: welded joints; fatigue assessment; structural stress

Spectra analysis and temperature measure of plasmas in YAG-MIG hybrid welding of 5A90 GUO Li[1], DUAN Aiqin[2], YU Yousheng[1] (1. School of Material Science and Engineering, Wuhan University of Technology, Wuhan 430023, China; 2. National Key Laboratory of High Energy Density Beam Processing Technology, Beijing Aeronautic Manufacturing Technology Research Institute, Beijing 100024, China). p106—108

Abstract: The spectra of vapor/plasmas were acquired by spectrometer during YAG-MIG hybrid welding of 5A90 Al-Li alloys in our research. The temperature values of the vapor/plasmas were calculated by the methods of relative intensity. The effects of arc current and heat input on the temperature of the vapor/plasmas were discussed. The results show that the spectra of hybrid welding in the range of 350—850 nm is mainly argon ion spectra line accompanied with a few Mg and Li ion. An average temperature under a set of processing parameters is 6554 K; compared to YAG welding, the value has an increase of 1200 K; however, it is near to the average temperature of MIG welding.

Key words: YAG-MIG hybrid welding; metal vapor/plasmas; spectrum

3-D numerical simulation of welding spherical valve core DING Hui, LEI Junxiang, ZHU Hanhua, LI Xinran (University of Shanghai for Science and Technology, Shanghai 200093, China). p109—112

Abstract: Welding is the key course in manufacturing the spherical valve core through steel tube's necking, assembling, welding and grinding. Because the necked workpiece is under stress before welding and is to be prepared for grinding after welding, how to choose sound welding parameters so as to control residual stress with the precondition of excellent weld quality becomes the focus of this paper. A series of numerical simulations which show the real-time dynamic changes under different welding parameters for necked workpiece are demonstrated, and the optimization parameters are obtained through comparing the welding size and residual stress after welding. Analysis and illustrations on the accumulated results show that the residual stress after welding is overlapped in the former procedures.

Key words: spherical valve core; necking; numerical simulation; parameter optimization